HYDROGEOLOGY JOURNAL

Electronic Supplementary Information for

Explaining long-range fluid pressure transients caused by oilfield wastewater disposal using the hydrogeologic principle of superposition

Ryan M. Pollyea

Department of Geosciences, Virginia Polytechnic Institute and State University, Blacksburg, VA, USA

Correspondence: rpollyea@vt.edu

Contents

S1. Introduction

Supplemental Information contained in this file includes simulation results for three additional permeability scenarios (Figure S1) tested as part of this study. For each supplemental permeability scenario, oilfield wastewater is simulated in a one-quarter model domain for (i) a single injection well operating at 2,080 m^3 day^{-1} (13,000 bbl day^{-1}) and (ii) a well field comprising nine injection wells on a 6 km regular grid with each well operating at 2080 m^3 day^{-1} $well^{-1}$ (13,000 bbl day^{-1} $well^{-1}$) (Figures S2 – S4). To further illustrate how the principle of superposition drives long-range pressure accumulation, Movie S1 presents a short animation of simulation results within a detailed section of the primary nine-well model scenario shown in Figure 5 of the main article. This animation shows that pressure fronts radiating from closely spaced injection wells merge and locally increase the hydraulic gradient, the result of which drives fluid pressure to much larger lateral distances than is possible from isolated injection wells.

S2. Code Selection and Governing Equations

The code selection for this study is TOUGH3 (Jung et al., 2017) compiled with equation of state module EOS7 for simulating non-isothermal mixtures of pure water and brine with mixing by advective transport and molecular diffusion. The TOUGH3 simulator solves the governing equations for mass and heat flow with parallel numerical solvers (PetSc), which allows for extremely high-resolution numerical simulation. The complete solution scheme for TOUGH3 is presented in the TOUGH3 User's Guide (Jung et al., 2018), and summarized in the context of fully saturated flow here.

The generalized integral form of the mass and energy conservation equation is written as:

$$\frac{d}{dt}\int_{V_n} M^\kappa dV_n = \int_{\Gamma_n} \mathbf{F}^\kappa \cdot \mathbf{n} d\Gamma_n + \int_{V_n} q^\kappa dV_n. \quad \text{(S1)}$$

In this formulation, the left side of Equation S1 is the accumulation term, where M represents a mass (or energy) component κ, which for this study are water, brine and energy (in which case κ is specific inner energy). As a result, the time-change of mass (or energy) within closed volume V_n is equivalent to the sum of (i) the integral component flux ($\mathbf{F}^\kappa$) normal to the volume-bounding surface (Γ_n) and (ii) any sources or sinks (q^κ) of component κ within V_n. The mass accumulation term in Equation S1 is generalized as:

$$M^\kappa = \phi \sum \rho X^\kappa \quad \text{(S2)}$$

where, ϕ is porosity, ρ is fluid density, X^κ is the fraction of mass component κ. In Equation S2, M^κ is summed over all fluid phases occupying pore space in V_n; however, this study only considers fully saturated flow so the phase partition is not considered. For energy conservation, the heat accumulation term is given by:

$$M^\kappa = (1-\phi)\rho_R C_R T + \phi \sum S \rho u \quad \text{(S3)}$$

where, ρ_R is rock density, C_R is rock specific heat, T is temperature, and u is fluid enthalpy. In TOUGH3, the advective flux ($\mathbf{F}^\kappa|_{adv}$) for each mass component κ is given as $\mathbf{F}^\kappa|_{adv} = \sum X^\kappa \mathbf{F}$, where $\mathbf{F}$ is presented here in terms of Darcy's Law for fully saturated porous media:

$$\mathbf{F} = -\frac{k}{\mu}(\nabla \mathbf{P} - \rho \mathbf{g}) \quad \text{(S4)}$$

In Equation S4, k is intrinsic permeability, μ is dynamic viscosity, P is fluid pressure, and $\mathbf{g}$ is the vector of gravitational acceleration. Diffusive mass transport ($\mathbf{f}^\kappa$) is modeled as

$$\mathbf{f} = -\phi \rho \mathbf{D}^\kappa \nabla X^\kappa \quad \text{(S5)}$$

where, $\mathbf{D}^\kappa$ is the diffusion coefficient for mass component κ. The models developed here consider wastewater disposal wells as source terms in the relevant grid cells. To convert from volume rate (Q) to mass rate ($\dot{m}$), the standard conversion, $\dot{m} = Q\rho$, is implemented, where ρ is the injection fluid density at reservoir temperature and pressure.

To simulate the effects of variable density brine, this study implements the TOUGH3 equation of state module, EOS7, for aqueous, nonisothermal mixtures of pure water and brine (Pruess et al., 2012). In this formulation, aqueous phase salinity is accounted for on the basis of a brine mass fraction, X_b, for which density and viscosity are interpolated between endmembers comprising pure water and brine. The density of the water-brine mixture (ρ_m) for variable brine saturation (X_b) is approximated as

$$\frac{1}{\rho_m} = \frac{1-X_b}{\rho_w} + \frac{X_b}{\rho_b} \quad \text{(S6)}$$

where, ρ_w is the density of pure water and ρ_b is the density of a reference brine when X_b is 1. For this study, the reference brine density is 1,123 kg m^{-3}, which corresponds with produced brine from the Mississippi Lime formation (TDS ≈ 207,000 ppm at 40°C and 21 MPa). The approximation for density of the brine-water mixture (Equation S6) assumes the compressibility of brine to be the

same as for pure water. To account for the effects of pressure, temperature, and salinity on the viscosity of the brine-water mixture (μ_m), the polynomial correction by Herbert et al. (1988) is invoked as:

$$\mu_{\mathrm{m}}(P,T,X_{\mathrm{b}}) = \mu_{\mathrm{w}}(P,T)\left[1 + 0.4819X_{\mathrm{b}} - 0.2774X_{\mathrm{b}}^2 + 0.7814X_{\mathrm{b}}^3\right] \qquad \text{(S7)}$$

where, μ_w is the viscosity of pure water, for which temperature and pressure dependence is accounted for by internally referencing the equation of state for water at each timestep. In TOUGH3, the governing equations are solved by the integral finite difference method for space discretization, while time discretization is a fully implicit, first-order backward finite difference. This results in a coupled, nonlinear set of equations that are solved simultaneously by Newton-Raphson iteration.

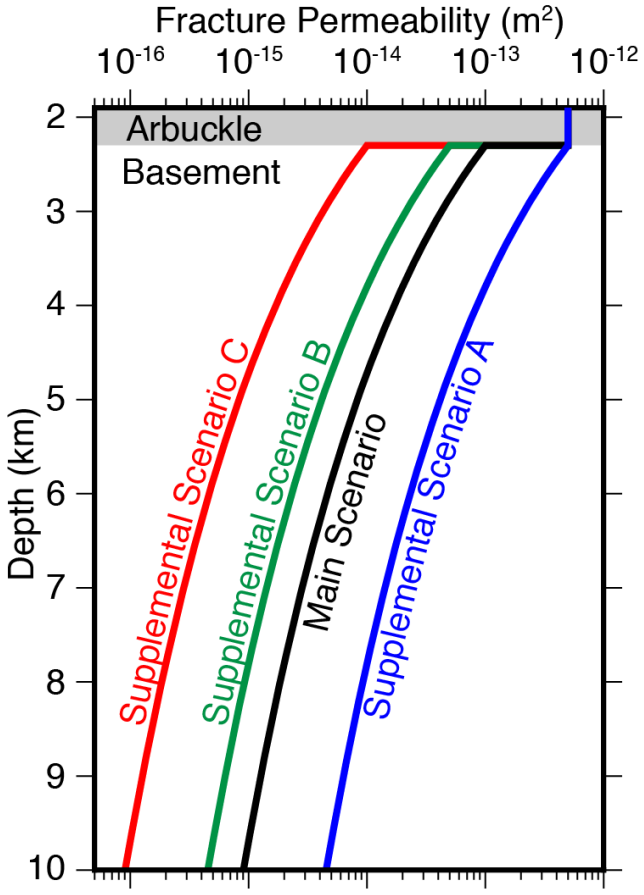

Figure S1. Due to the uncertainty that is inherent to basement permeability, four depth-decaying permeability scenarios were tested for this study. The main scenario (black) line is described in the main article text. Supplemental Scenario A (blue) is one-half order of magnitude (OM) higher than the main scenario. Supplemental Scenarios B (green) and C (red) are one-half and one OM lower than the main scenario, respectively.

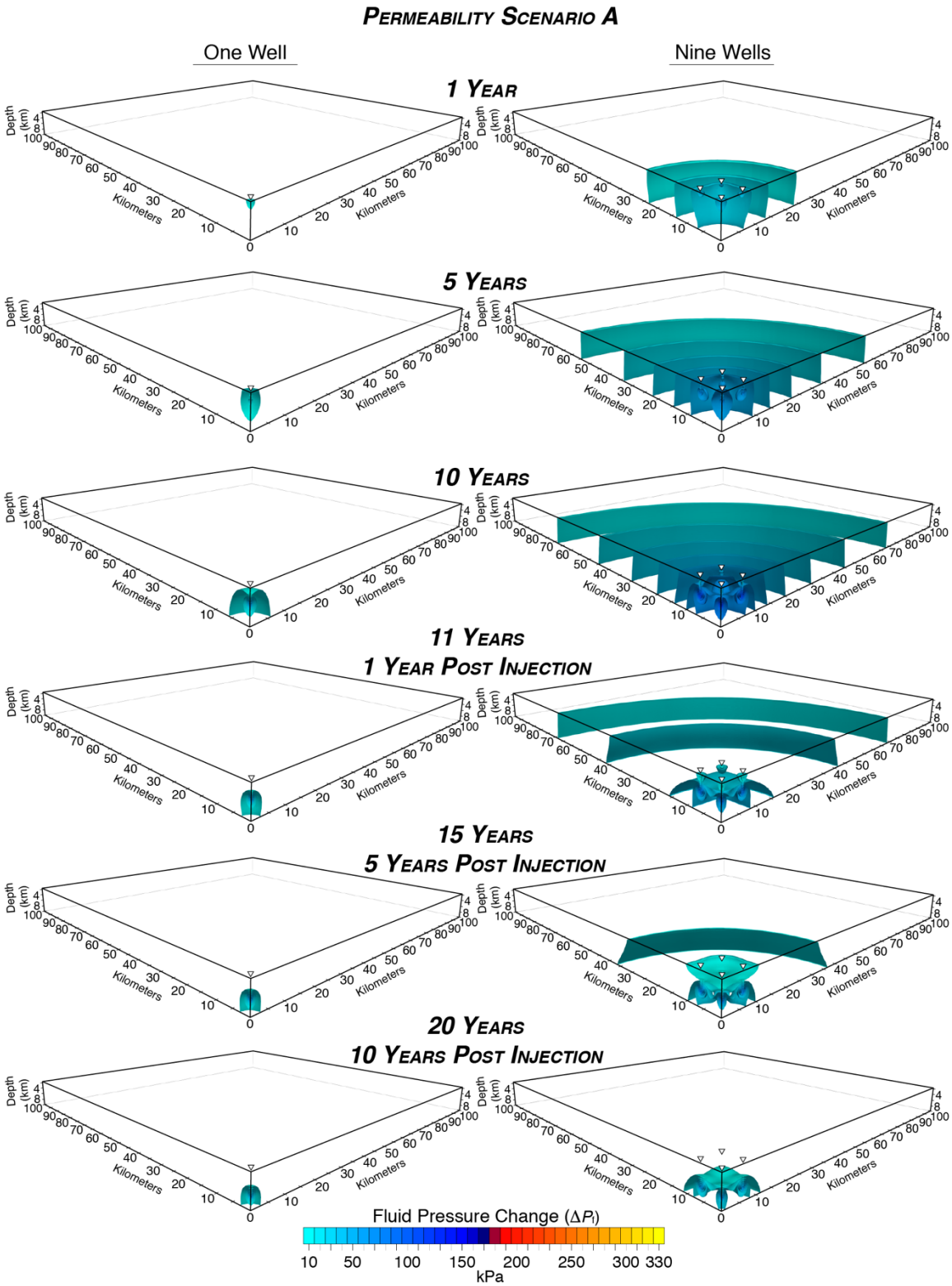

Figure S2. Complete simulation results for Permeability Scenario A (Figure S1, blue). Results are shown as isosurface contours of fluid pressure above initial conditions (ΔP_f) in 10 kPa intervals.

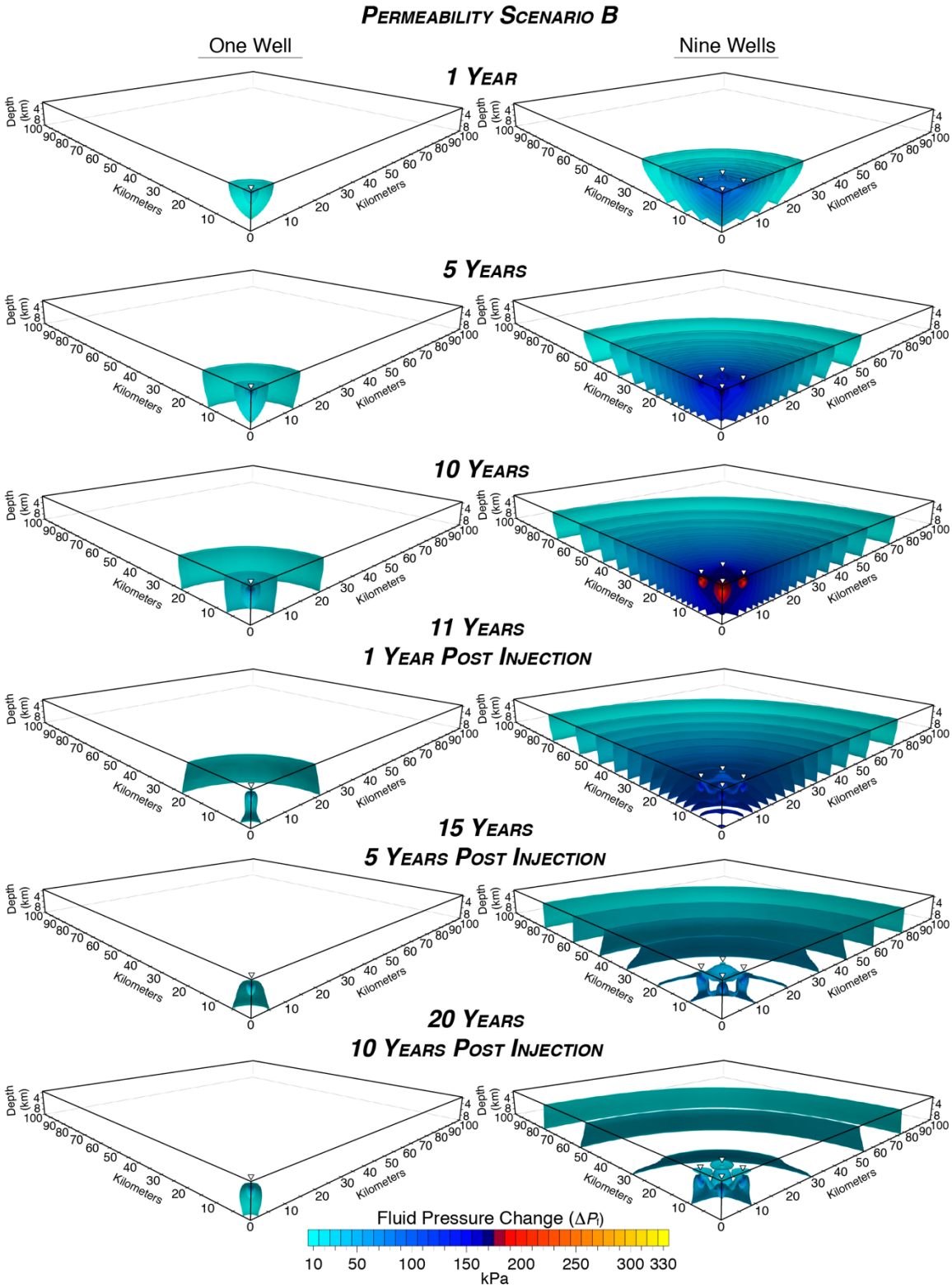

Figure S3. Complete simulation results for Permeability Scenario B (Figure S1, green). Results are shown as isosurface contours of fluid pressure above initial conditions (ΔP_f) in 10 kPa intervals.

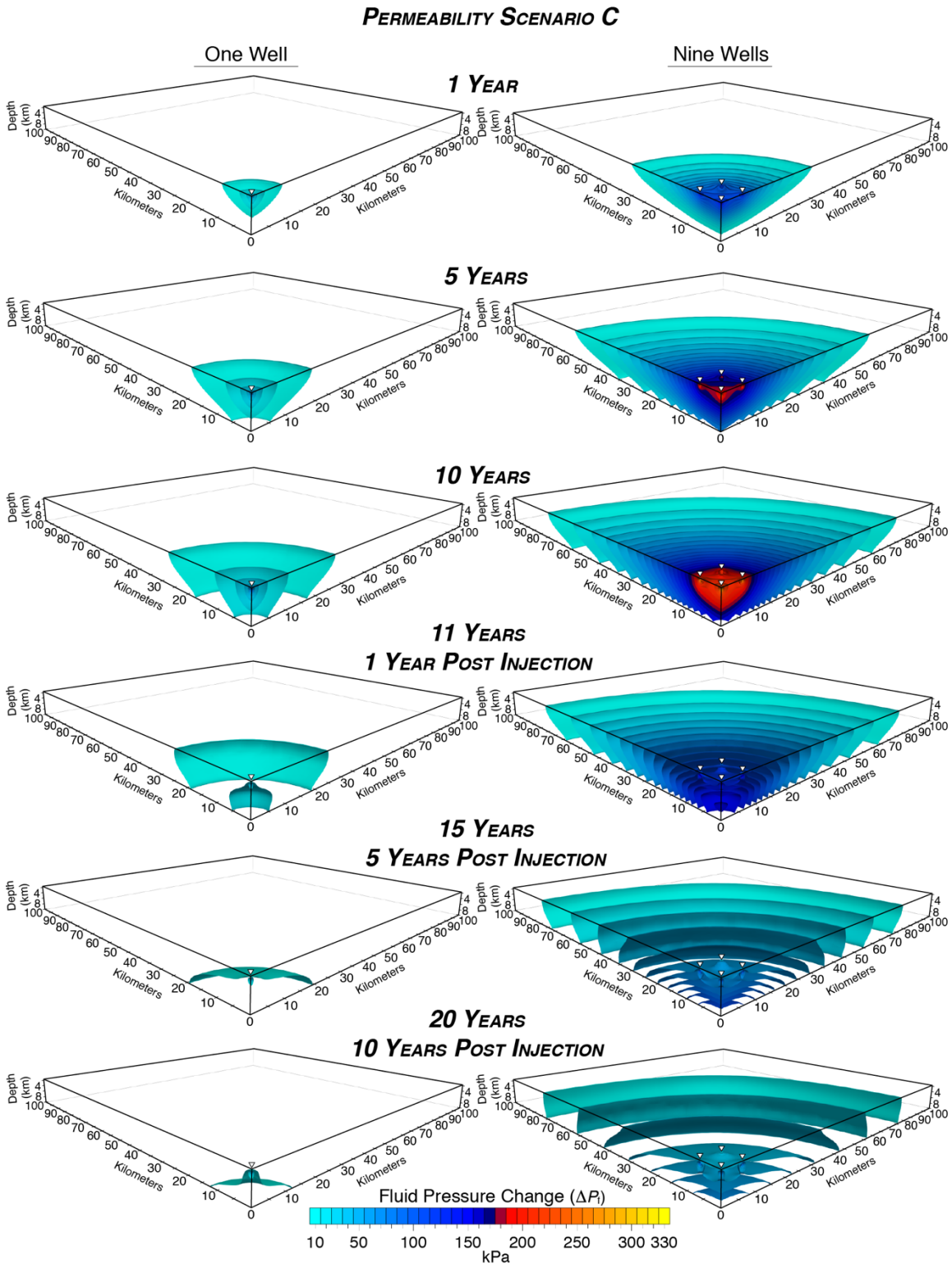

Figure S4. Complete simulation results for Permeability Scenario C (Figure S1, red). Results are shown as isosurface contours of fluid pressure above initial conditions (ΔP_f) in 10 kPa intervals.

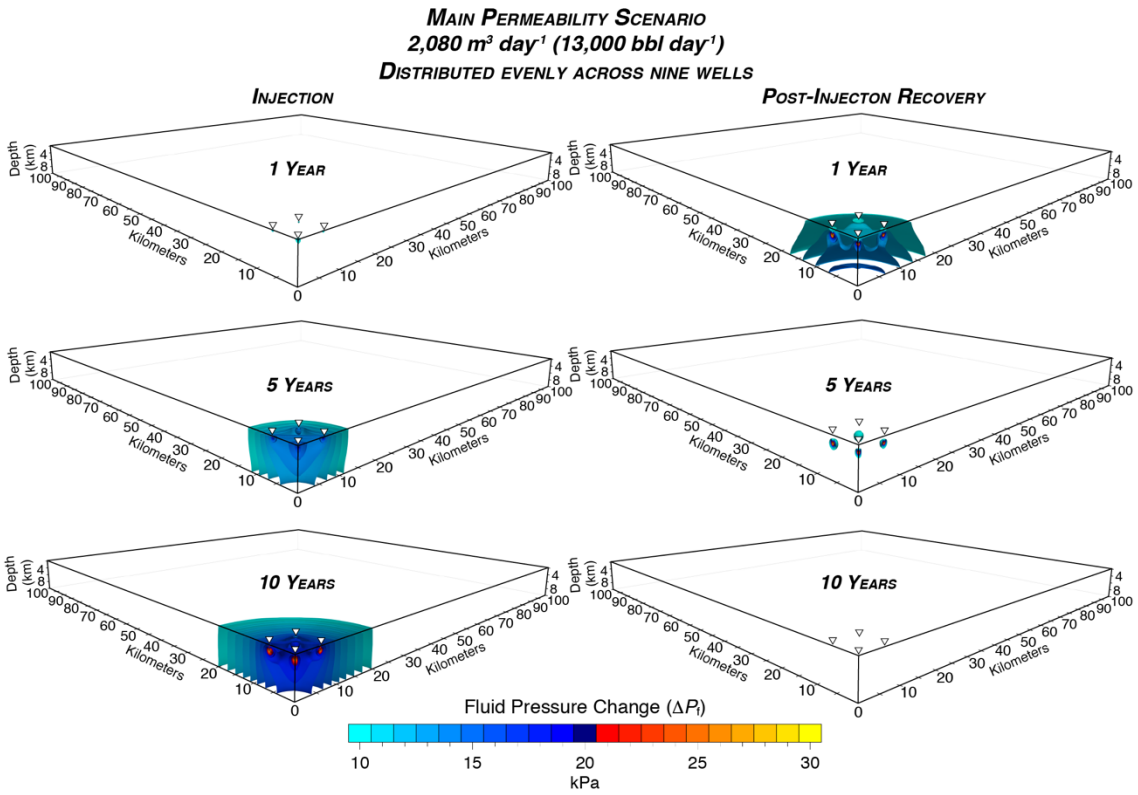

Figure S5. Simulation results for the main permeability scenario (Figure S1, black) when a total injection rate of 2,080 m^3 per day (13,000 bbl day^{-1}) is distributed evenly across nine injection wells. The total injection rate for each well is 231 m^3 day^{-1} (1,444 bbl day^{-1}). Results are shown as isosurface contours of fluid pressure above initial conditions (ΔP_f) from 10 to 30 kPa in 1 kPa contour intervals. Simulation invokes four-fold symmetry and only a ¼-domain is simulated.

Movie S1. Animated simulation results of the detailed section presented in Figure 5 of the main article. This animation illustrates the hydrogeologic principle of superposition as a temporal process. Results are for the period between 3 and 10 years of oilfield wastewater disposal. Isosurface contours of pressure accumulation (ΔP_f) above hydrostatic pressure are shown in 10 kPa intervals. The effects of superposition are easily recognized at 7 years of simulation as the ΔP_f isosurface connecting $x = y = 7$ km merges with the corresponding pressure front radiating from the injection well at $x = y = 6$ km. The additive effects of superposition drive fluid pressure fronts to substantially longer radial distances from well clusters than from individual wells.

The movie (.mpg) is provided as separate ESM.

ESM References

Herbert, A., Jackson, C., Lever, D. (1988) Coupled groundwater flow and solute transport with fluid density strongly dependent on concentration, *Water Resources Research,* Vol. 24, p. 1781 - 1795.

Jung, Y., Pau, G. S. H., Finsterle, S., & Pollyea, R. M. (2017) TOUGH3: A new efficient version of the TOUGH suite of multiphase flow and transport simulators. *Computers & Geosciences*. v. 108, p. 2-7, November. doi:10.1016/j.cageo.2016.09.009.

Jung, Y., Pau., G., Finsterle, S., and Doughty, C. (2018) *TOUGH3 User's Guide: Version 1.0*, Tech. Rep. LBNL-2001093 Lawrence Berkeley National Laboratory, January. Available online at: http://tough.lbl.gov/assets//files/Tough3/TOUGH3_Users_Guide_v2.pdf

Pruess,K. Oldenburg, C., and Moridis, G. (2012) *TOUGH2 User's Guide Version 2,* Tech. Rep. LBNL-43134 Lawrence Berkeley National Laboratory. Available online at: http://tough.lbl.gov/assets/docs/TOUGH2_V2_Users_Guide.pdf